ACS APPLIED MATERIALS & INTERFACES

Letter

www.acsami.org

Particle-Nested Inverse Opal Structures as Hierarchically Structured Large-Scale Membranes with Tunable Separation Properties

Do Kyung Rhee,[†] Bokyung Jung,[‡] Young Hun Kim,[†] Seon Ju Yeo,[†] Se-Jin Choi,[§] Ali Rauf,[†] Sungsoo Han,[‡] Gi-Ra Yi,[†] Daeyeon Lee,[∥] and Pil J. Yoo*[,†]

[†]School of Chemical Engineering and SKKU Advanced Institute of Nanotechnology (SAINT), Sungkyunkwan University, Suwon 440-746, Korea

[‡]Advanced Materials Research Center, Samsung Advanced Institute of Technology (SAIT), Yongin 446-712, Korea

[§]MCNet Co., Ltd., Gunpo 435-833, Republic of Korea

[∥]Department of Chemical and Biomolecular Engineering, University of Pennsylvania, Philadelphia, Pennsylvania 19104, United States

Supporting Information

ABSTRACT: A novel multiscale porous architecture where an individual particle is nested inside a hollow chamber of inverse-opal (IO) frame is created using a large scale self-assembly of core−shell structured colloidal particles and subsequent selective removal of the outer shells of the colloids. Since the nested particle is smaller than the size of individual IO chamber, the interconnected nanochannels are spontaneously formed within the structured frame. The size of internal nanochannels is readily tuned to have high permeability and size-selective separation capability, which is successfully tested for nanoparticle separation.

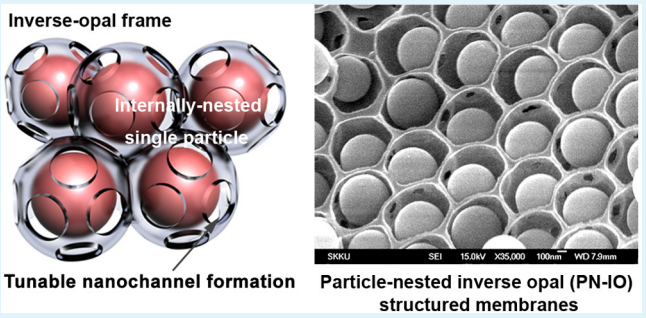

KEYWORDS: *inverse-opal, core−shell, nanochannels, membranes, separation*

Precise control over the three-dimensional structure of porous materials enables the quantitative investigation of their structure−property relationship.[1] Among various approaches, the use of three-dimensional inverse opal (3D-IO) structures based on self-assembled templates of colloidal particles offers the distinct advantages of being simple and highly scalable. Their outstanding structural regularity as well as high porosity and specific surface area make these IO structures highly desirable for applications ranging from photonic devices to electrode materials.[2−7]

Recent advances in the fabrication of IO structures include efforts to embed secondary nanostructures inside the primary IO frame, generating hierarchical structures with added physical properties. For example, the hollow chambers within IO structures can be coated by means of the layer-by-layer assembly of polyelectrolyte multilayers, or can be filled with ensembles of nanoparticles; these processes can be readily carried out by infiltration of materials through the interconnected pores.[8,9] However, many of these methods undesirably disrupt the intrinsic interconnectivity of the primary IO phase, significantly compromising the most unique structural feature and thus properties of the IO structure. Therefore, if the structural properties of the secondary nanostructures could be elaborately introduced without sacrificing the pore interconnectivity of the original IO frame, such a material would be useful as a hierarchical porous material, particularly for membrane applications.[10,11] Moreover, precise control over the three-dimensional structure of the 3D-IO frame and their structural regularity provide a unique opportunity to develop a profound understanding on the structure−performance relationship of hierarchically structured membranes.

To introduce a secondary structure inside the primary IO template without disrupting the cell interconnectivity, an individual object that has a comparable shape and size to that of a unit hollow chamber could be implanted within the IO frame. However, when the embedded species is smaller than the size of the interconnecting pore, such objects cannot remain confined inside single chambers; rather, these objects will randomly aggregate by freely moving through the interconnected hollow IO chambers, making it unlikely that the resulting system will retain structural regularity. In contrast, if an object to be embedded is larger than the interconnecting pores, then steric effects will prevent its introduction into the primary structure. In either case, problems are likely to arise from the use of implantation processes to introduce secondary structures into the primary IO structure.

To overcome these limitations and create IO structures that retain pore connectivity and structural hierarchy, we present herein a novel means of employing particles of core−shell

Received: May 14, 2014
Accepted: June 16, 2014
Published: June 16, 2014

 © 2014 American Chemical Society dx.doi.org/10.1021/am5029654 | ACS Appl. Mater. Interfaces 2014, 6, 9950−9954

structure as a primary assembling unit for the opal phase (Figure 1a). After preparing an IO-structured frame around the

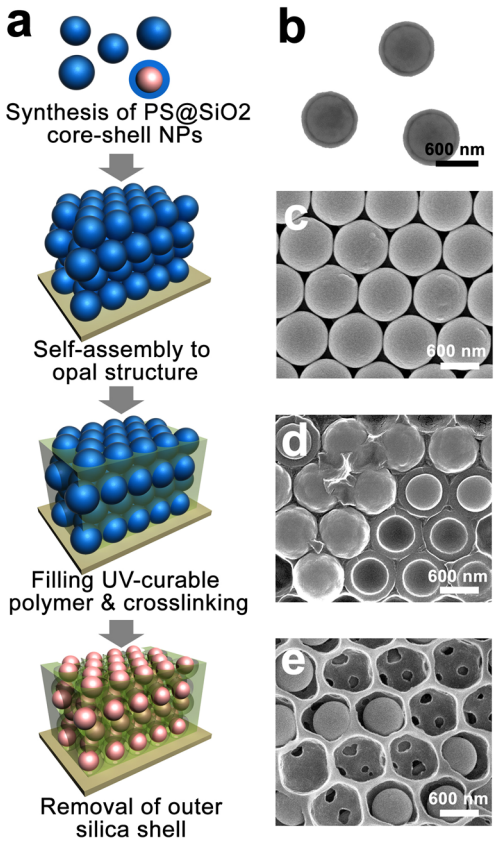

Figure 1. (a) Schematic of the procedure for fabricating the PN-IO structure. (b) Synthesis of core–shell structured monodisperse particles of PS@SiO_2. (c) Self-assembly of PS@SiO_2 particles to form the opal phase. (d) Formation of an IO frame via precursor infiltration and subsequent UV cross-linking. (e) Formation of the final PN-IO structure after selective removal of the outer SiO_2 shells. (b) Transmission electron micrograph and c–e are scanning electron micrographs (SEM).

particles using a UV-curable polymer, the outer shells of the assembled particles are selectively dissolved, thereby forming a hierarchical structure, in which each hollow chamber of the IO structure carries a single particle. In this manner, a secondary structure can be nested inside the primary IO structure over a large scale without compromising structural stability and porosity. Hereafter, we call this structure a particle-nested inverse opal (PN-IO). A similar structure of double-inverse-opal was previously reported; however, the localized ordering has only been used for switching the photonic bandgap.[12]

One notable feature of PN-IO is that a uniform nanoscale void gap between the nested particle and the surrounding wall is created; this gap can be further engineered through size tuning to function as well-defined nanochannels. The effective pore size can be controlled readily by adjusting the structural parameters of the core–shell particles or those of the IO-structured template. Because the interconnectivity of the macropores of the IO remains intact, the nanochannels between nested particles and pore walls are also interconnected to each other, making these structures suitable for membrane separations. In contrast to conventional membranes of which the effective pore size is empirically measured and adjusted, the proposed PN-IO structured membranes afford tunability over the accurate dimension of this nanoscale gap in a deterministic manner. Moreover, the high structural regularity and size uniformity of the nanochannels is greatly helpful for establishing the structure–property relationship in hierarchically porous membranes, potentially enabling membrane performance enhancement.[13]

To ensure the structural regularity of PN-IO materials, the self-assembled opal phase of the primary colloidal particles must first be constructed; success in doing so depends on various processing conditions, such as solvent evaporation rate, environmental temperature, relative humidity, and interactions with the underlying substrates.[5,14,15] However, using colloidal particles that are monodisperse in size is the most important factor in the assembly process. Hence, the core–shell colloidal particles should be synthesized to have minimal variation in size and shape. Another requirement is that the outer shells should be selectively removable to create the secondary nanochannel inside the IO frame, without deteriorating the internal colloidal core or the surrounding wall. In this regard, the use of a polymeric core with a sacrificial inorganic shell would be desirable, creating a large difference in solubility between the core and the shell to enable selective etching.

To synthesize monodisperse core–shell particles, we chose the system of a polystyrene core and a SiO_2 shell (PS@SiO_2), which allows fairly large scale generation with fine control over the SiO_2 shell thickness.[16−20] During the formation of the core–shell structure, surfactant molecules of polyvinylpyrrolidone (PVP) were adsorbed to the surface of the grown PS core, thereby creating a surface with carbonyl groups. Then, strong hydrogen bonding occurred between carbonyl groups and subsequently supplied hydroxyl groups of the SiO_2 precursor, eventually forming core–shell particles.[21] The PS core was synthesized using ammonium persulfate (APS) as an initiator, and was subsequently coated with a SiO_2 shell using vinyltrimethoxysiliane (VTMS) as a precursor.[22] In particular, as shown in Figure 1b, this pair offers the advantage of uniform control over the SiO_2 shell thickness simply by varying the concentration of the VTMS. The resulting monodisperse PS@SiO_2 colloidal particles of 420 nm in radius were self-assembled to form opal structures (Figure 1c). Subsequently, a UV-curable resin of poly(urethane acrylate) (PUA) was infiltrated through the voids inside the opal-structured template to form an encompassing IO frame (Figure 1d). Finally, using a selective solvent of dilute hydrofluoric acid (HF), the outer shell of SiO_2 was removed, thereby creating the PN-IO structures (Figure 1e). Details of the experimental procedures are provided in the Supporting Information, part 1.

Because the colloidal opal phase stems from face-centered cubic (FCC) stacking of particles, in which each particle has 12 nearest neighbors, 12 interconnecting pores accordingly are generated in the unit cell of the IO structure. In PN-IO structures, each internally nested colloidal particle is smaller than the hollow chamber; thus, the interconnecting pores of the IO frame remain open. At the same time, it should be noted that there exists a narrow void gap between the nested colloid particle and the surrounding IO frame. As shown in Figure 2a and 2b, the size of the residual void can be readily controlled by varying the size of the PS core particles. Minimal volumetric shrinkage of UV-curable PUA resin upon cross-linking (2–7%) enables the formation of large-scale membranes (size = 35 × 25 mm^2, thickness ~20 μm) without development of macroscale defects or cracks (Figure 2c).

dx.doi.org/10.1021/am5029654 | ACS Appl. Mater. Interfaces 2014, 6, 9950–9954

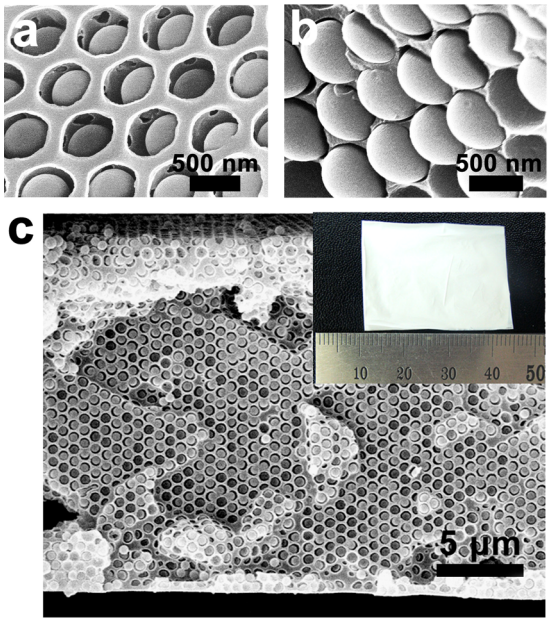

Figure 2. SEM observation of PN-IO structures. (a) PN-IO formed by using a core/shell ratio of 0.75 (concentration of VTMS = 400 mM). (b) PN-IO formed by using a core/shell ratio of 0.92 (concentration of VTMS = 90 mM). (c) Cross-sectional observation of a large-scale PN-IO structure (inset: 35 × 25 mm^2). Thickness of the free-standing membrane film is 20 μm.

Structural characteristics of the PN-IO can be quantitatively analyzed using a geometric model, as shown schematically in Figure 3a. Assuming the unit structure in which an individual particle is placed inside a hollow IO chamber, one can define the size of the nanochannels that spontaneously form between the colloidal particle and the wall of the IO frame. By introducing spherical coordinates within the confined unit geometry of the PN-IO, the effective width of the nanochannels can be estimated as follows (see the Supporting Information, part 2)

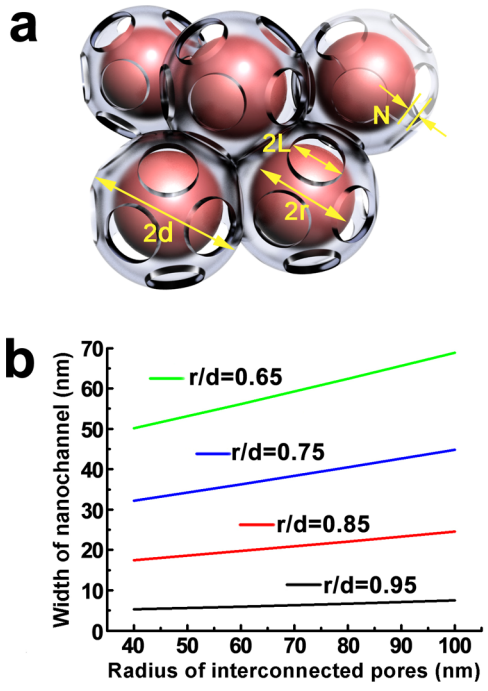

Figure 3. (a) Simplified unit geometry of the PN-IO structure. Nanochannel width (N) can be estimated as a function of other structural variables. (b) Estimated nanochannel width as a function of the core/shell ratio of the colloidal particles (r/d) and the interconnected pore size of the IO frame (L).

$$N = \sqrt{X_n^2 + Y_n^2 + (Z_n - (d - r))^2} - d$$

$$X_n = -r\sin(\arccos(-\sqrt{6}/3) + L/r)\,\frac{1}{2\sin(\arccos(-\sqrt{6}/3))}$$

$$Y_n = r\sin(\arccos(-\sqrt{6}/3) + L/r)\,\sin\left(\arccos\left(\frac{-1}{2\sin(\arccos(-\sqrt{6}/3))}\right)\right)$$

$$Z_n = r\cos(\arccos(-\sqrt{6}/3) + L/r) \quad (1)$$

where N is the effective width of the nanochannels, and r, d, and L are the radii of the internally nested colloid, the hollow IO chamber, and the interconnecting pores of the IO structure, respectively. As can be seen in eq 1, the size of nanochannels can be tuned by varying the relative ratio of r and d or by varying L. In experiments, the ratio of r/d was controlled through the shell thickness of the PS@SiO_2 colloidal particles, and L could be controlled through the formulation of the PUA resin. For example, when a relatively highly shrinkable PUA (with a greater degree of cross-linking) was used to form the IO frame, ~ 200 nm sized interconnecting pores were created. In contrast, when a less shrinkable PUA resin was used, the resulting diameter of the interconnecting pores decreased to ~90 nm (see the Supporting Information, part 3).[23]

To better understand the key processing parameters in controlling the size of the nanochannels, we investigated the effect of r/d and L on the estimated nanochannel size. As illustrated in Figure 3b, the nanochannel size responds sensitively to variation in the core/shell ratio (r/d) of the particles used. In contrast, the influence of the interconnecting pore size (L) is observed to be less significant. In the case of a fixed interconnecting pore size of 120 nm in a PN-IO structure (radius of individual chamber = 420 nm), the effective diameter of nanochannel is expected to vary from 50 to 5 nm in response to varying the core−shell ratio from 0.65 to 0.95.

To experimentally test the membrane performance of the PN-IO, we first measured the pure water permeability of PN-IOs as a function of the core/shell ratios of the PS@SiO_2 colloidal particles (Figure 4a). When ~10 nm-sized narrow nanochannels were generated by using particles with a core/shell ratio of 0.92, a relatively low permeability of 60 L/(m^2 h bar) (LMH/bar) was obtained, whereas an enhanced permeability of 240 LMH/bar was observed for ~28 nm sized nanochannels resulting from the use of particles with the core/shell ratio of 0.8. As shown in Figure 4a, the permeability through the interconnected nanochannels generally seems to follow the Hagen−Poiseuille relationship, in which the flux value is proportional to the square of the nanochannel size (i.e., the effective pore area)

$$J = \frac{\varepsilon\pi N^2}{8\mu\delta\tau}\Delta P \quad (2)$$

dx.doi.org/10.1021/am5029654 | ACS Appl. Mater. Interfaces 2014, 6, 9950−9954

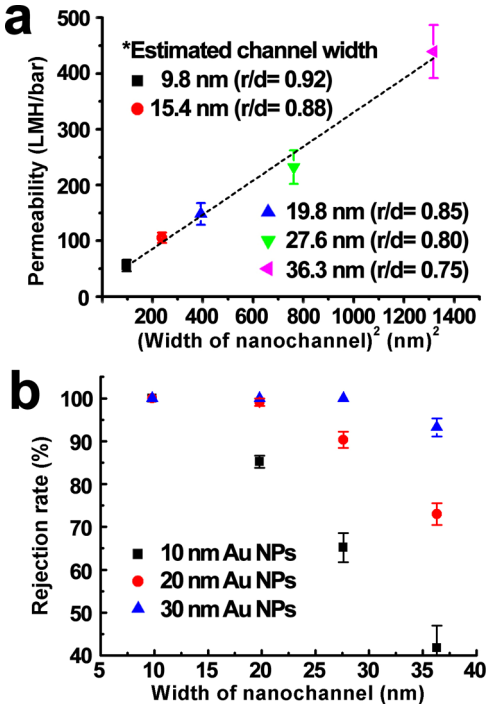

Figure 4. (a) Measured pure water permeability versus estimated nanochannel area. Permeate flux was measured under 1-bar-pressurized condition. (b) Rejection rate of Au nanoparticles by PN-IO structured membranes with varying estimated nanochannel widths.

where J is the volumetric flux, ε is the surface porosity, N is the average pore radius, μ is the viscosity, δ is the membrane thickness, τ is the tortuosity, and ΔP is the pressure drop across the membrane. Notably, the permeability of the PN-IO structured membranes was comparable to that of conventional membranes; for example, the pure water permeability for a commercial membrane with effective pore diameter of 25 nm (VSWP02500, Millipore) is approximately 100 LMH/bar. Also, the prepared membranes were mechanically stable up to a 3-bar-pressurized condition without causing any burst or compaction problem.

Finally, the size-exclusion separation of the PN-IO structured membranes was investigated through the selective removal of nanoparticles (Figure 4b). Au nanoparticles with different sizes (10, 20, and 30 nm in diameter) were filtered through the membranes with different nanochannel sizes. When the estimated size of nanochannels was smaller than the Au nanoparticles, rejection rates greater than 98% were obtained through the size-exclusion effect (the small amount of particle penetration might be partly due to a slight deviation in the size monodispersity of the Au nanoparticles used). In the case of Au nanoparticles that were smaller than the size of nanochannels, it was observed that fairly good separation efficiency was retained (greater than 60%). This could be attributed to the structural characteristics of the three-dimensionally architectured membranes, which could allow for the removal of particles by an adsorption mechanism.

In conclusions, we have presented a novel approach to fabricate a hierarchically porous architecture in the form of PN-IO structures, and further investigated the feasibility of their application as high-performance ultrafiltration membranes. To create PN-IO structures, monodisperse core−shell colloidal particles were synthesized and subsequently processed to form the IO structured frame, and then the outer shells of the colloids were selectively removed. The resulting multiscale porous structures had pore size tunability ranging from several to tens of nanometers, and were tested for nanoparticle filtration. In particular, because of the highly uniform structural regularity and excellent pore interconnectivity of the PN-IO, they acted as mesoporous membranes with high separation efficiency. We believe the exquisite design and extended functionality of the PN-IO structure will be useful as a platform technology for next-generation membrane materials.

■ ASSOCIATED CONTENT

Supporting Information

Details of experimental procedures, mathematical derivation of the effective width of the void nanochannels, and formulation variation of UV-curable prepolymer. This material is available free of charge via the Internet at http://pubs.acs.org.

■ AUTHOR INFORMATION

Corresponding Author

*E-mail: pjyoo@skku.edu.

Notes

The authors declare no competing financial interest.

■ ACKNOWLEDGMENTS

This work was supported by research grants of NRF (2012S1A2A1A01031215), Global Frontier R&D Program on Center for Multiscale Energy System (2012M3A6A7055540), and Basic Science Research Program (2010-0027955) funded by the National Research Foundation under the Ministry of Science, ICT & Future, Korea. D.L. acknowledges support from the NSF (DMR-1055594).

■ REFERENCES

(1) Wu, D.; Xu, F.; Sun, B.; Fu, R.; He, H.; Matyjaszewski, K. Design and Preparation of Porous Polymers. *Chem. Rev.* **2012**, *112*, 3959−4015.

(2) Yu, X.; Lee, Y.-J.; Furstenberg, R.; White, J. O.; Braun, P. V. Filling Fraction Dependent Properties of Inverse Opal Metallic Photonic Crystals. *Adv. Mater.* **2007**, *19*, 1689−1692.

(3) Lee, K. T.; Lytle, J. C.; Ergang, N. S.; Oh, S. M.; Stein, A. Synthesis and Rate Performance of Monolithic Macroporous Carbon Electrodes for Lithium-Ion Secondary Batteries. *Adv. Funct. Mater.* **2005**, *15*, 547−556.

(4) Esmanski, A.; Ozin, G. A. Silicon Inverse-Opal-Based Macroporous Materials as Negative Electrodes for Lithium Ion Batteries. *Adv. Funct. Mater.* **2009**, *19*, 1999−2010.

(5) Ahn, S. H.; Chi, W. S.; Kim, D. J.; Heo, S. Y.; Kim, J. H. Honeycomb-Like Organized TiO_2 Photoanodes with Dual Pores for Solid-State Dye-Sensitized Solar Cells. *Adv. Funct. Mater.* **2013**, *23*, 3901−3908.

(6) Kim, H.-N.; Moon, J. H. Enhanced Photovoltaic Properties of Nb_2O_5-coated TiO_2 3D Ordered Porous Electrodes in Dye-sensitized Solar Cells. *ACS Appl. Mater. Interfaces* **2012**, *4*, 5821−5825.

(7) Kumoda, M.; Watanabe, M.; Takeoka, Y. Preparations and Optical Properties of Ordered Arrays of Submicron Gel Particles: Interconnected State and Trapped State. *Langmuir* **2006**, *22*, 4403−4407.

(8) Yeo, S. J.; Kang, H.; Kim, Y. H.; Han, S.; Yoo, P. J. Layer-by-layer Assembly of Polyelectrolyte Multilayers in Three-dimensional Inverse Opal Structured Templates. *ACS Appl. Mater. Interfaces* **2012**, *4*, 2107−2115.

(9) Cho, C.-Y.; Moon, J. H. Hierarchically Porous TiO_2 Electrodes Fabricated by Dual Templating Methods for Dye-Sensitized Solar Cells. *Adv. Mater.* **2011**, *23*, 2971−2975.

(10) Wang, X.; Husson, S. M.; Qian, X.; Wickramasinghe, S. R. Inverse Colloidal Crystal Microfiltration Membranes. *J. Membr. Sci.* **2010**, *365*, 302−310.
(11) Wang, X.; Husson, S. M.; Qian, X.; Wickramasinghe, S. R. Inverse Colloidal Crystal Ultrafiltration Membranes. *Sep. Purif. Technol.* **2012**, *93*, 33−41.
(12) Ruhl, T.; Spahn, P.; Hermann, C.; Jamois, C.; Hess, O. Double-Inverse-Opal Photonic Crystals: the Route to Photonic Bandgap Switching. *Adv. Funct. Mater.* **2006**, *16*, 885−890.
(13) Krieg, E.; Weissman, H.; Shirman, E.; Shimoni, E.; Rybtchinski, B. A Recyclable Supramolecular Membrane for Size-selective Separation of Nanoparticles. *Nat. Nanotechnol.* **2011**, *6*, 141−146.
(14) Stein, A.; Wilson, B. E.; Rudisill, S. G. Design and Functionality of Colloidal-Crystal-Templated Materials − Chemical Application of Inverse Opal. *Chem. Soc. Rev.* **2013**, *42*, 2763−2803.
(15) Retsch, M.; Jonas, U. Hierarchically Structured, Double-Periodic Inverse Composite Opals. *Adv. Funct. Mater.* **2013**, *23*, 5381−5389.
(16) Schmid, A.; Fujii, S.; Armes, S. P. Polystyrene-Silica Nanocomposite Particles via Alcoholic Dispersion Polymerization using a Cationic Azo Initiator. *Langmuir* **2006**, *22*, 4923−4927.
(17) Lu, Y.; McLellan, J.; Xia, Y. Synthesis Crystallization of Hybrid Spherical Colloids Composed of Polystyrene Cores and Silica Shells. *Langmuir* **2004**, *20*, 3464−3470.
(18) Chen, M.; Zhou, S.; Wu, L.; Xie, S.; Chen, Y. Preparation of Silica-Coated Polystyrene Hybrid Spherical Colloids. *Macromol. Chem. Phys.* **2005**, *206*, 1896−1902.
(19) Graf, C.; Vossen, D. L. J.; Imhof, A.; van Blaaderen, A. A General Method to Coat Colloidal Particles with Silica. *Langmuir* **2003**, *19*, 6693−6700.
(20) Deng, T.-S.; Zhang, Q.-F.; Zhang, J.-Y.; Shen, X.; Zhu, K.-T.; Wu, J.-L. One-step Synthesis of Highly Monodisperse Hybrid Silica Spheres in Aqueous Solution. *J. Colloid Interface Sci.* **2009**, *329*, 292−299.
(21) Leng, W.; Chen, M.; Zhou, S.; Wu, L. Capillary Force Induced Formation of Monodisperse Polystyrene/Silica Organic − Inorganic Hybrid Hollow Spheres. *Langmuir* **2010**, *26*, 14271−14275.
(22) Deng, T.; Marlow, F. Synthesis of Monodisperse Polystyrene@Vinyl-SiO_2 Core-Shell Particles and Hollow SiO_2 Spheres. *Chem. Mater.* **2012**, *24*, 536−542.
(23) Yoo, P. J.; Choi, S.-J.; Kim, J. H.; Suh, D.; Baek, S. J.; Kim, T. W.; Lee, H. H. Unconventional Patterning with a Modulus-Tunable Mold: from Imprinting to Microcontact Printing. *Chem. Mater.* **2004**, *16*, 5000−5005.